Accepted Manuscript

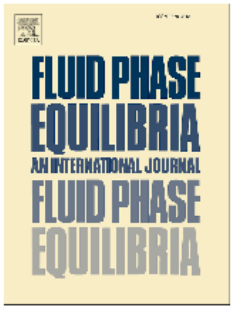

Effects of ionic hydration and hydrogen bonding on flow resistance of ionic aqueous solutions confined in molybdenum disulfide nanoslits: Insights from molecular dynamics simulations

Yumeng Zhang, Wei Zhu, Jiahui Li, Yudan Zhu, Anran Wang, Xiaohua Lu, Wei Li, Yijun Shi

PII: S0378-3812(19)30060-3

DOI: https://doi.org/10.1016/j.fluid.2019.02.012

Reference: FLUID 12100

To appear in: *Fluid Phase Equilibria*

Received Date: 28 August 2018

Revised Date: 21 January 2019

Accepted Date: 9 February 2019

Please cite this article as: Y. Zhang, W. Zhu, J. Li, Y. Zhu, A. Wang, X. Lu, W. Li, Y. Shi, Effects of ionic hydration and hydrogen bonding on flow resistance of ionic aqueous solutions confined in molybdenum disulfide nanoslits: Insights from molecular dynamics simulations, *Fluid Phase Equilibria* (2019), doi: https://doi.org/10.1016/j.fluid.2019.02.012.

Effects of ionic hydration and hydrogen bonding on flow resistance of ionic aqueous solutions confined in molybdenum disulfide nanoslits: Insights from molecular dynamics simulations

Yumeng Zhang [a], Wei Zhu [a], Jiahui Li [a], Yudan Zhu [a,*], Anran Wang [a], Xiaohua Lu [a], Wei Li [b], Yijun Shi [c]

[a] *College of Chemical Engineering, State Key Laboratory of Materials-oriented Chemical Engineering, Nanjing Tech University, Nanjing 211816, PR China*

[b] *European Bioenergy Research Institute (EBRI), Aston Institute of Materials Research (AIMR), Aston University, Birmingham, B4 7ET, England, UK*

[c] *Division of Machine Elements, Luleå University of Technology, Luleå 97187, Sweden*

*To whom correspondence should be addressed.

Contact information:

Yudan Zhu ydzhu@njtech.edu.cn

ABSTRACT: Single-layer molybdenum disulfide (MoS_2) is a novel two-dimensional material that has attracted considerable attention because of its excellent properties. In this work, molecular dynamics simulations were performed to investigate the effect of different kinds of alkali metal ions (Li^+, Na^+, and K^+) on the flow resistance of ionic aqueous solutions confined in MoS_2 nanoslits under shearing. Three slit widths (*i.e.* 1.2, 1.6, and 2.0 nm) were investigated. Simulation results showed that the friction coefficient followed the order of $K^+ < Na^+ < Li^+$. The friction coefficient decreased with the increasing of slit width. Unique confined spatial distributions of different types of ionic aqueous solutions led to different confined ionic hydrations for different cations. These differences lead to different orientations of surrounding water molecules and then form different hydrogen bond (HB) networks. The friction coefficient was greatly dependent on the number of HBs per water; *i.e.*, the larger the number of HBs formed, the lower was the flow resistance.

Keywords: MoS_2, ionic aqueous solutions, molecular simulations, flow resistance, nanoconfinement

1. Introduction

Single-layer molybdenum disulfide (MoS_2), which is a novel two-dimensional material, has attracted considerable attention because of its excellent properties [1-3]. For example, Cao *et al.* [4] found that spreading single-layer MoS_2 on a nanodevice surface significantly decreased friction and minimized the effects of humidity on the device performance. MoS_2 has promising applications in areas such as nanopore DNA sequencing [5, 6], supercapacitor electrodes [7], and desalination membranes [8]. Most of these applications essentially involve ionic aqueous solutions confined within the restricted nanospaces of MoS_2. Flow resistance generated by the relative motion between the ionic aqueous solution and the MoS_2 interface greatly affects the overall performance. The reduction of flow resistance of common ionic aqueous solutions (e.g. Li^+, Na^+, and K^+ aqueous solutions) under nanoconfinement is therefore a key factor in the design and application of MoS_2-based nanomaterials [9].

Classical macroscopic theories of fluids flow are not applicable, when describing the flow resistance of ionic aqueous solutions at the nanoscale. The main reason is that the effect of the interactions between fluid molecules and the solid wall usually is not be considered into these theories. Under confinement within spaces of several molecular sizes, however, these interactions (primarily steric interactions/hydration, van der Waals interactions, and electrostatic interactions [10]) make significant contributions to the fluid flow behaviors. For this reason, many anomalous experimental phenomena at the nanoscale have been reported. For example, Wu *et al.* used a novel *in situ* nuclear magnetic resonance technique to show non-neutral specific enrichment of ionic aqueous solutions confined in non-charged hydrophobic carbon slits of size 1 nm [11]. Sakuma *et al.* performed shear resonance experiments

to less than 1 nm [12]. These phenomena demonstrated that the interfacial properties greatly influence the behaviors of confined ions.

MoS_2 is hydrophilic in nature. To date, the mechanism of flow resistance reduction of ionic aqueous solutions confined in hydrophilic nanospace has not been completely understood. Gaisinskaya-Kipnis *et al.* [13] recently used a surface force balance to study the flow resistance of different hydrated alkali metal ions (Li^+, Na^+, and K^+) confined on hydrophilic mica surfaces. The results showed that the friction coefficient of Li^+ was higher than that of K^+. Given that the bulk hydration ability of Li^+ is stronger than that of K^+, interestingly, their findings contrast with the expectation of *hydration lubrication* theory [14]. According to the *hydration lubrication* theory, the stronger the ionic hydration is, the lower the flow resistance. The theory is usually used in explaining the mechanisms of friction coefficient reduction for ionic aqueous solutions at the nanoscale. Based on the above findings, we speculated that the mechanism of resistance reduction of (Li^+, Na^+, and K^+) aqueous solutions confined in hydrophilic MoS_2 nanoslits appears to be more associated with other microstructures of solution than ionic hydration.

Molecular simulation is a powerful tool for investigating the flow resistance at liquid–solid interfaces under nanoconfinement. Zhang *et al.* used non-equilibrium molecular dynamics (NEMD) simulations to study the effects of solvent polarity on the flow resistance of a nanoconfined fluid and found that the flow resistance was greatly dependent on the solvent polarity [15]. Wang *et al.* reported that the special ordered structures formed by water molecules on a solid surface could effectively reduce the flow resistance between water molecules and interfaces [16]. On the other hand, molecular simulation also plays a significant role in analyzing the unique microstructures of nanoconfined fluids. He *et al.* used molecular simulations to observe the effects of the presence of ions on nanoscale friction between surfaces

surface and the number of hydration water molecules [17]. Summers and co-workers carried out a series of molecular simulation studies on frictional properties of alkylsilane monolayers on SiO_2 surfaces. The results showed that friction coefficient was related with surface-induced the global orientational ordering and density of the monolayers [18-20]. For this reason, we were inclined to utilize NEMD simulation to explore the underlying relationship between the fluid microstructures and flow resistance.

In this work, we focused on studying the effects of alkali metal cations (Li^+, Na^+, and K^+) with different hydration strengths on the flow resistance of ionic aqueous solutions confined in MoS_2 nanoslits. These effects are important for further applications of MoS_2-based nanomaterials, because most of them essentially involve ionic aqueous solutions confined within the restricted nanospaces of MoS_2. We have addressed the following questions: (I) How do the flow resistances of different ionic aqueous solutions differ from each other? (II) How does the slit width affect the flow resistance for the same ionic aqueous solution? (III) What are the underlying contributions to the confined ionic flow resistance at the molecular level? Through NEMD simulation, we determined that the influences of slit width and ion characteristics on friction coefficients are reflected by the change in the HB networks of water molecules. We also explored various other ideas, such as variations in the water density profile, or in ionic hydration numbers. However, the HB network provided the clearest understanding of the variation in the friction coefficients.

2. Simulation models and method

The simulation model is shown in Fig. 1. The slit model consisted of two monolayer MoS_2 slabs in a periodic simulation box. The size of the monolayer MoS_2 slab was 4.43 × 3.11 × 0.32 nm^3 ($X \times Y \times Z$). Three ionic aqueous solutions (LiCl,

L^{-1}, which is widely used in molecular simulation studies on the behavior of ionic aqueous solutions [21-24]. A 1.0 nm vacuum layer was reserved on both sides of the slabs to avoid interactions between the upper and lower slab molecules caused by the periodic repeat. Previous research indicated that confined ionic aqueous solutions can show unique behaviors that differ greatly from those of their bulk counterparts, especially when the confinement size is less than several nanometers [10]. Three slit widths, *i.e.*, 1.2, 1.6, and 2.0 nm (labeled d12, d16, and d20), were therefore investigated in this work.

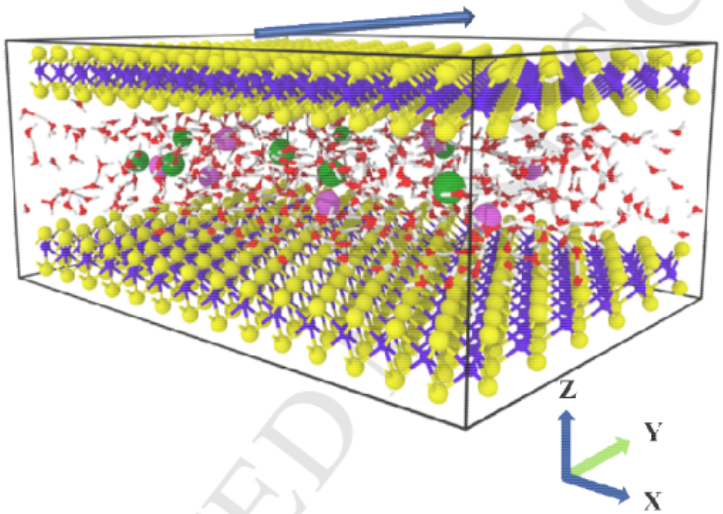

Fig. 1. Model of ionic aqueous solution confined in a MoS_2 slit. The yellow and blue atoms represent the sulfur and molybdenum atoms in MoS_2 molecules, respectively. The red and white atoms represent the oxygen and hydrogen atoms in water molecules, respectively. The green and pink atoms represent the cation and anion atoms, respectively.

The LAMMPS software package was used for all simulations [25]. The SPC/E water model [26] was chosen and OPLS-AA field parameters were used for ions [27]. The force field developed by Varshney *et al.* [28] was used; this was recently used by

The non-bonded interactions between atoms were treated as a combination of Lennard-Jones and coulombic pairwise interactions, defined as

$$U(r_{ij}) = 4\varepsilon_{ij}[(\frac{\sigma_{ij}}{r_{ij}})^{12} - (\frac{\sigma_{ij}}{r_{ij}})^{6}] + \frac{q_i q_j}{r_{ij}} \quad (1)$$

In equation (1), ε_{ij} and σ_{ij} represent energy and size parameters, respectively, and follow the geometric mixing rule.

The following steps were used to determine the number of fluid molecules in slits given that slits with different widths have different capacities for accommodating fluid molecules. (I) Two single-layer MoS_2 slabs with a certain width were placed in a water box (11 nm × 3.2 nm × 3 nm) with a density of 1.0 g × cm^{-3} along the *X* and *Y* directions. (II) After energy minimization, 1.0 ns molecular dynamics (MD) simulations were performed to obtain the equilibrium state of water molecules by applying the isobaric–isothermal (NPT) ensemble only along *X* direction [30]. The number of fluid molecules in the slit was stable. The system temperature was held constant at 300 K and the pressure was set as 100 bar to avoid the appearance of nanobubbles. (III) Afterward, water molecules outside the slit were removed and replaced with ions to obtain the solution concentration of 1.0 mol L^{-1}. The ions and retained water molecules confined inside the slit were used as the initial configuration for the following NEMD."

The flow resistances of different ionic aqueous solutions under non-equilibrium conditions were investigated by performing 15 ns NEMD simulations with integral steps of 1.0 fs, using a canonical (NVT) ensemble. The upper slab moved along the *Y*-axis at a constant speed of 50 m s^{-1}. The coordinates were saved every 1.0 ps and those for the last 10 ns were used for further analysis. The Nosé–Hoover [31] thermostat was coupled with fluid molecules at 300 K. A cutoff of 1.0 nm was used to

calculated using the particle–particle particle–mesh solver [32]. Periodic boundary conditions were implemented in all three directions.

Table 1

Force field parameters used in this work.

Site	ε, kcal mol^{-1}	σ, nm	q, e
Mo	19.329	0.255	+0.7600
S	1.397	0.337	-0.3800
Li^+	0.01828	0.213	+1.000
Na^+	0.00277	0.333	+1.000
K^+	0.00033	0.494	+1.000
Cl^-	0.11783	0.442	-1.000
O	0.1554	0.317	−0.8476
H	0.000	0.000	+0.4328

3. Results and discussion

The friction coefficient was used to evaluate the effects of different alkali metal ions on the flow resistance of ionic aqueous solutions confined in MoS_2 nanoslits of different widths (section 3.1). The density distributions of water molecules and ions confined in MoS_2 nanoslits were studied to explain the variations in the friction coefficients (section 3.2). Finally, the microstructures of confined fluid molecules, including ionic hydration and HB structures, were analyzed to clarify the underlying mechanisms at the molecular scale (section 3.3). The results showed that the friction coefficients results were attributed to cations and wall effects on HB structures. Flow resistance was low when a large number of HBs had formed. The following sections provide a detailed analysis.

evaluation of flow resistance [33]. The friction coefficient is defined as the ratio of the frictional force to the normal force exerted on the surface of the bottom slab. The bottom slab keeps fixed during the simulations. The frictional force includes the lateral interaction between all the atoms of the bottom slab and aqueous solution. Zhang *et al*. used a similar method for calculating friction coefficients [15]. The friction coefficients of various ionic aqueous solutions confined in slits of different widths were calculated.

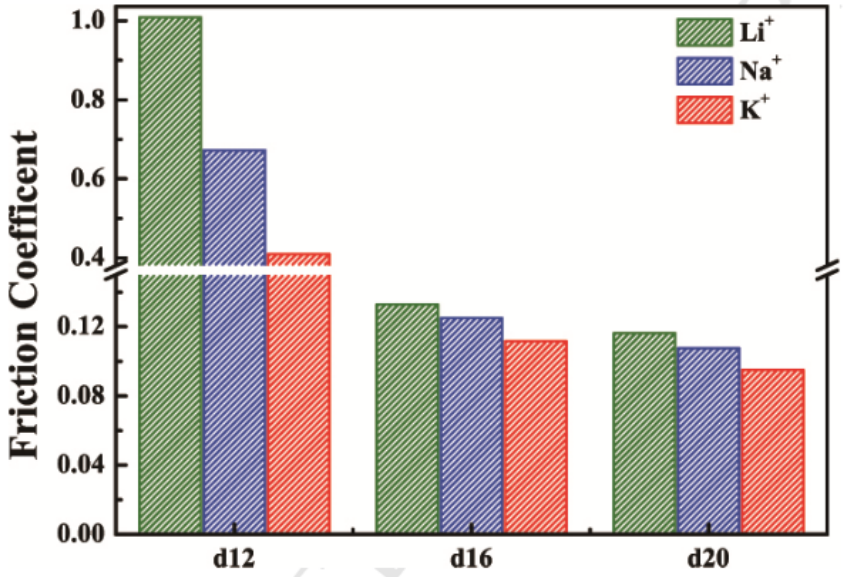

Fig. 2. The friction coefficients of Li^+, Na^+ and K^+ aqueous solutions confined within MoS_2 slits with different widths. The d12, d16 and d20 on the horizontal axis represent the slits with 1.2, 1.6 and 2.0 nm widths, respectively.

Fig. 2 shows that for the three cations, the friction coefficient decreases with increasing slit width. This dependence of the friction coefficient on the slit width is in line with the results of our previous study of water molecules confined in TiO_2 slits [34]. The friction coefficient for d12 is much higher than those for d16 and d20. This phenomenon could be associated with the distributions and microstructures of fluid molecules confined in slits. (This will be further analyzed in sections 3.2 and 3.3) For

The results here are contrary to those expected on the basis of the *hydration lubrication* theory. Li^+ has the highest friction coefficients, and they are 2.47, 1.19, and 1.12 times higher than those of K^+ (which had the lowest friction coefficients) for d12, d16, and d20, respectively. This indicates that a narrower slit has a greater impact on the friction coefficients of different alkali metal ions. In addition, we studied the effect of the moving speed of the upper slab on the value of the friction coefficient in d12 (Fig. S1). As illustrated in Fig. S1, the friction coefficients exhibited the same trends under different speeds. Nevertheless, the values of the friction coefficient drastically decreased as speed decreased. The friction coefficients of water molecules confined within TiO_2 slits showed similar dependences on speed [34].

3.2 Density distributions of water molecules and ions confined in MoS_2 nanoslits

3.2.1 Density distributions of water molecules

The distributions of ionic aqueous solutions in slits were determined by analyzing the density distributions [$\rho(z)/\rho_0$] of water molecules in three types of ionic aqueous solutions along the Z direction (perpendicular to the surface), as shown in Fig. 3. The density profiles of oxygen atoms were used to characterize those of water molecules, because the oxygen atom is near the center of mass of a water molecule.

The density distributions of water molecules in the three ionic aqueous solutions are almost identical for slits with the same width. And they are similar to those of pure water confined in other hydrophilic nanoslits [30, 33-34]. This indicates that the presence of ions does not affect the spatial distributions of water molecules. Leng *et al.* [35] reported that the density distributions of water molecules in 1 M KCl aqueous solution confined in mica slits of width 2.3 nm were the same as those of pure water under the same conditions. Water molecules in the three slits are distributed symmetrically in the axial direction relative to the center (at Z = 0.0 nm), and the

layer) from the surfaces, and the density of water molecules near the central axis is close to that of the bulk. However, the water molecules in d12 form two peaks at a distance of 0.31 nm (first layer) from the surface, and there is a pronounced water peak at the central axis (second layer). This observation suggests that d12 are more tightly bound to water molecules than the other two slits, making the water molecules less mobile. This is why the friction coefficients for d12 are much larger than those for d16 and d20.

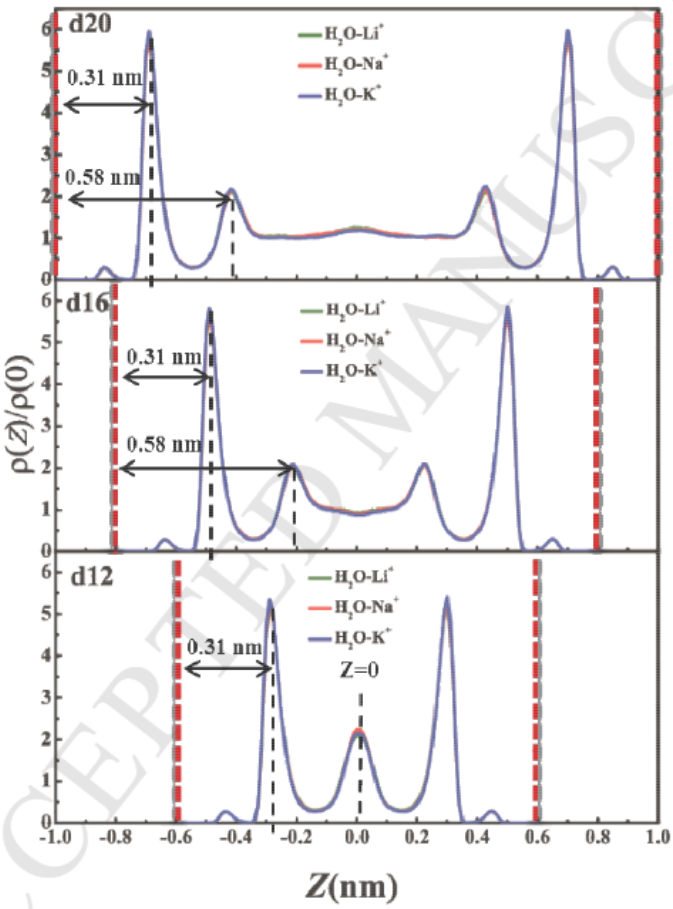

Fig. 3. Density profiles of water molecules in Li^+, Na^+ and K^+ aqueous solutions confined in d12, d16 and d20 along the *Z* direction. The red dashed lines represent the surfaces of slits.

3.2.2 Density distributions of cations

distributions are almost identical for slits of the same width. The reason for this was investigated by analyzing the two-dimensional density distributions of cations in the X–Z direction. In Fig. 4, a brighter color means a greater density. The Z ranges of Li^+, Na^+, and K^+ confined in d12, d16, and d20 are listed in Table 2.

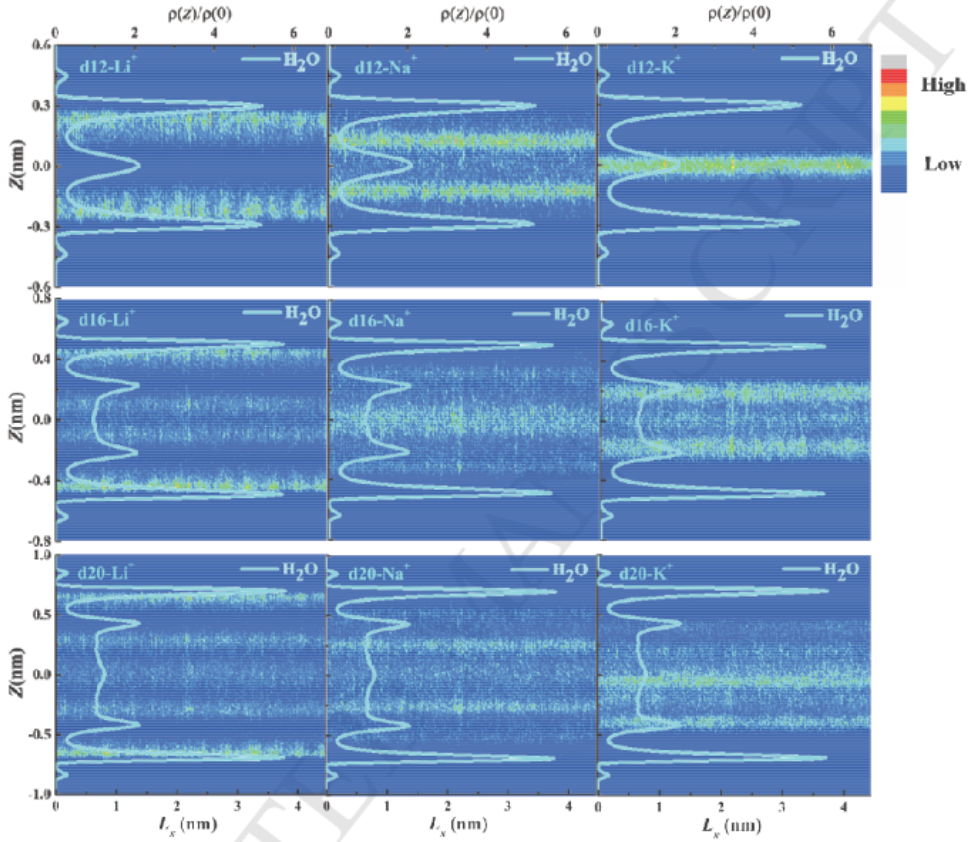

Fig. 4. X–Z planar density distributions of Li^+, Na^+ and K^+ confined in d12, d16 and d20. The light blue curve shows the density distributions of water molecules. Horizontal coordinates (bottom) represent the lateral distance along the X direction of the slits. The density distributions of water molecules (light blue curve) are drawn together to illustrate the relative position of cation distribution. The horizontal coordinates (upper) represent the magnitudes of the water density profiles.

Fig. 4 shows that for d12 Li^+ and Na^+ both form two symmetrical bright regions at the central axis, whereas K^+ forms only one bright region at the center. This indicates

222 layer of water molecules. Compared with Li^+, Na^+ is closer to the central axis and is
223 located between the first and second layers of water molecules. Unlike the other two
224 ions, K^+ overlaps with the second layer of water molecules. To clarify the reason for
225 the differences in density distribution in terms of energy, we analyzed the potential of
226 mean force (PMF) profiles along the *Z* direction for Li^+, Na^+ and K^+. The detailed
227 analysis is described in the supplementary materials.

228 **Table 2**

229 The *Z*-ranges of Li^+, Na^+ and K^+ confined in d12, d16 and d20.

Ions	*Z*-ranges, nm		
	d12	d16	d20
Li^+	(-0.28, -0.12) (0.12, 0.28)	(-0.49, -0.39) (0.39, 0.49) (-0.15, 0.15)	(-0.67, -0.57) (0.57, 0.67) (-0.34, 0.34)
Na^+	(-0.19, -0.06) (0.06, 0. 19)	(-0.35, 0.35)	(-0.54, 0.54)
K^+	(-0.06, 0.06)	(-0.26, 0.26)	(-0.44, 0.44)

230 For d16 and d20, Li^+ forms three symmetrical bright regions at the central axis,
231 whereas Na^+ and K^+ form only one bright region at the center. Li^+ is the closest cation
232 to the slit wall among the three ions. Li^+ not only partially overlaps with the first layer
233 of water molecules but also almost completely overlaps with bulk water molecules
234 located in the central region. Na^+ overlaps with the second layer of water molecules
235 and bulk water molecules. K^+ partially overlaps with the second layer of water
236 molecules and almost completely overlaps with bulk water molecules. The above
237 analysis shows that the distributions of the three cations are significantly different.
238 Each type of cation in d12 is clearly concentrated in one or two bright areas. For d16

speculated that the nature of the cation determines its preferential distribution in slits, and the slit width affects the degree of cation distribution. However, the spatial distributions of cations can cause variations in the microstructures of water molecules, which in turn affects the friction coefficient. A similar hypothesis was also proposed by Sakuma *et al*. [12]. They found experimentally that the distributions of Na^+ within mica nanoslits could affect the viscosity and pointed out that this is probably associated with the formation of two opposing Na^+ hydration layers. The microstructures of fluid molecules were further analyzed to clarify the underlying mechanism; the results are discussed in section 3.3.

3.3 Microstructures analysis of fluid molecules nanoconfined within slits

3.3.1 Average effective hydration number of cations under the nanoconfinement

Ionic hydration is an important phenomenon and cannot be ignored when studying the behavior of nanoconfined ions [10, 36, 37]. The main difference among the three ionic aqueous solutions is the cation hydration strength, which follows the order $K^+ < Na^+ < Li^+$ in bulk ionic aqueous solutions. The effects of confinement on the extent of ionic hydration were evaluated by investigating hydration of cations confined in MoS_2 nanoslits.

Generally, the hydration number of an ion is regarded as the coordination number of the ion and can be calculated according to equation (2), where R_{min}, ρ, and $g_{io}(r)$ represent the first coordination shell radius, the water density, and the cation–oxygen radial distribution function, respectively. Based on the orientation distributions of water molecules around ions, our group previously proposed a new concept, namely the *hydration factor*, which showed that not all water molecules in the first coordination layer, but only those in a certain orientation, are hydrated [38]. According to the definition of the hydration factor, water molecules in the first

hydration microstructures better than the coordination number can [39, 40]; therefore, we determined the average effective hydration numbers of Li^+, Na^+, and K^+ in the slits. The effective hydration number of bulk ions was also calculated for comparison; the results are shown in Fig. 5.

$$N = 4\pi\int_0^{R_{\min}} r^2 \rho g_{i0}(r) dr \tag{2}$$

$$N_{eff} = N * \frac{N_{-1<\cos\alpha<-0.72}^{\text{first shell}}}{N_{\text{all}}^{\text{first shell}}} \tag{3}$$

Fig. 5 shows that the order of the average effective hydration number of nanoconfined ions is $Li^+ > Na^+ > K^+$; this is in accord with the hydration strengths in the bulk. However, the variations in the confined ionic hydration numbers for different cations are different from those in the bulk. The average effective hydration number of nanoconfined Li^+ is larger than that of bulk counterpart. This indicates that nanoconfinement can enhance the hydration of Li^+. For Na^+, there is little difference between the hydration numbers of nanoconfined and bulk ions, which indicates that nanoconfinement has little effect on the hydration of Na^+. In contrast to that of Li^+, the average effective hydration number of nanoconfined K^+ is clearly less than that in the bulk, which indicates that ionic hydration is weakened by confinement. It can therefore be concluded that the different responses of ionic hydration to nanoconfinement are caused by the preferred distributions of different cations.

Fig. 4 shows that some (d16 and d20) or even all (d12) of the Li^+ ions are concentrated near the first layer of water molecules, and partially overlap with this layer. Na^+ is distributed between two layers of water molecules (d12) or completely overlaps with the second layer and bulk of water molecules (d16 and d20). K^+ is always distributed at the center and partially covered by the second layer of water molecules. In terms of the hydration radius (0.265, 0.315, and 0.345 nm for Li^+, Na^+,

greater than those of the other ions. The effect of Na^+ on the two layers of water molecules is similar. K^+ mainly affects the second layer of water molecules and only part of the first layer of water molecules. Fig. 3 shows that water molecules tend to be concentrated near the wall, and the density of the first layer of water molecules is significantly higher than those of the others. The different responses of ionic hydration to nanoconfinement for the three cations therefore are the result of different effects of the cations on each layer of water molecules.

In general, the spatial distributions of cations and water molecules greatly contribute to the different confined ionic hydration behaviors of different cations. Given that the variations in ionic hydration inevitably influence HB network formation, the HB network structures were analyzed.

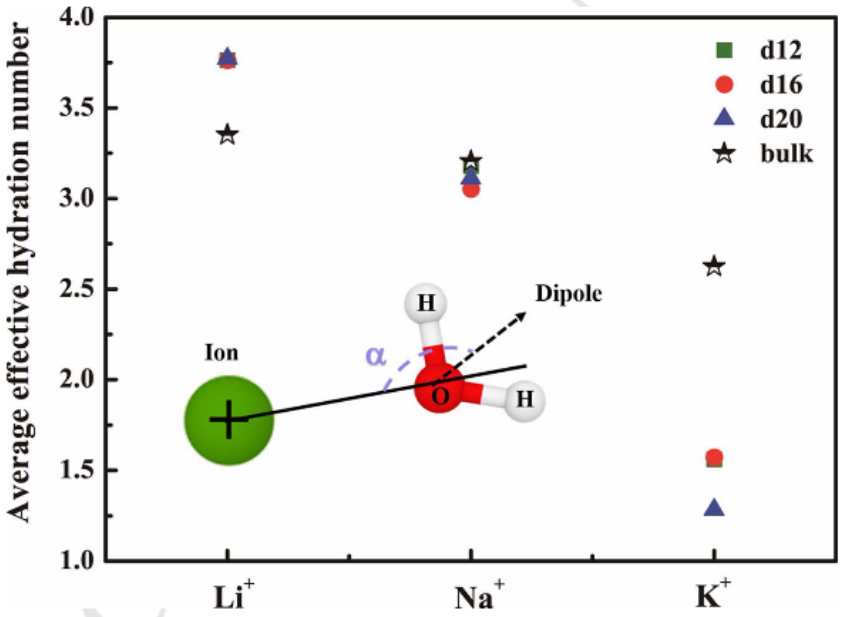

Fig. 5. Average effective hydration number of Li^+, Na^+ and K^+ confined in d12, d16 and d20. The black star represents the effective hydration number of the ions in bulk. The inset is a schematic of the orientation angle α of a water molecule around a cation.

3.3.2 Average number of hydrogen bonds in water molecules

Previous studies have shown that the water molecule structures in nanoslits have an important influence on fluid flow and liquid lubrication [41-43]. HB structure is the most important index that reflects the structures of water molecules [44, 45]. Fig. 6 shows the average number of HBs in water molecules (N_{HB}). An HB is formed between two water molecules (one acts as a donor and the other acts as an acceptor) when the following three criteria are simultaneously satisfied [46]. (I) The distance between the oxygen atoms in the donor and acceptor water molecules is less than 0.35 nm. (II) The distance between the oxygen in the acceptor and the hydrogen in the donor is less than 0.245 nm. (III) The O–H···O angle is less than 30°. The average HB number for pure water molecules in the bulk (black dashed line) is also shown in Fig. 6. The average HB number of water molecules in an ionic aqueous solution under nanoconfinement is less than that in pure bulk water. This indicates that both the interface and the ions may affect the HB structures of water molecules.

For the same slit, the order of the average HB number is $Li^+ < Na^+ < K^+$, indicating that the different confined ionic hydrations of the cations generate different degrees of damage to the HB networks. Li^+ has the greatest ability to destroy HB network structures of water molecules, whereas K^+ has the lowest ability. Other studies have shown that among these three ions, K^+ has the least destructive effect on the water structure [47, 48]. Similarly, for slits of different widths, the trend in the average HB number of water molecules in ionic aqueous solutions is d12 < d16 < d20, which indicates that stricter confinement makes HB network breakage easier.

In addition, we analyze the average number of hydrogen bonds of water layer by layer on the basis of the density distributions of water molecules (Fig. S3). The layered analysis is further verified the above results. As shown in Fig. S3(a), the sequence of N_{HB} for the water molecules in the first layer is $Li^+ < Na^+ < K^+$ for the three studied nanoslits. The same trend is also observed for the water molecules

sequence of N_{HB} for water molecules within the whole slit is also $Li^+ < Na^+ < K^+$ (Fig. 6). However, different layers had different N_{HB} values. The N_{HB} values of water molecules within the first layer are lower than those of the water molecules outside the first layer because the interaction between the surface and fluid molecules inhibit hydrogen bond formation among water molecules near the surface. The N_{HB} values of the water molecules outside the first layer range from 2.78 to 3.07, which are close to that of bulk water (3.15).

A combination of the analyses in sections 3.2 and 3.3.1 shows that the spatial distributions of cations and water in ionic aqueous solutions affect the confined ionic hydration behaviors. However, the hydration behaviors of confined ions can change the HB network structures of water molecules; this is similar to the results reported by Gallo *et al*. [49]. The hydration around confined cations orients the surrounding water molecules in a specific direction, which leads to formation of different HB networks. A greater average HB number means better stability of the fluid molecules. A combination of these results with those shown in Fig. 2 shows that the friction coefficient under confinement decreases with increasing number of HBs per water molecule. Mu *et al*. experimentally found that adding substances that easily form HBs to a lubricant improves the lubricating properties [50]. They proposed that the HBs played the dominant role in reducing the flow resistance. The simulation results here confirm their expectation and also explain the sequence of friction coefficients for different alkali metal ions at the molecular scale. It is therefore believed that HB structure is an important index for evaluating fluid flow resistance under nanoconfinement; *i.e.*, the more HBs formed, the lower is the flow resistance.

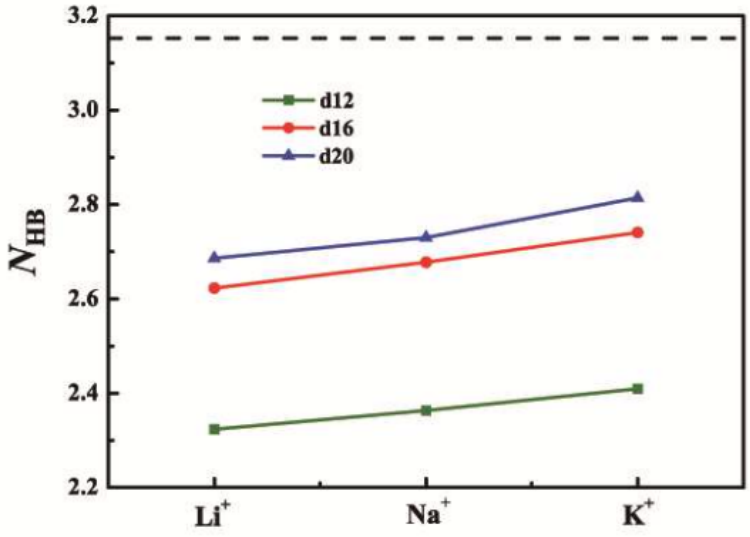

Fig. 6. Number of hydrogen bond per water molecule in Li^+, Na^+ and K^+ aqueous solutions confined within d12, d16 and d20. The dashline represents the value of pure water molecules in bulk.

4. Conclusion

In this work, NEMD simulations were used to study the effects of different alkali metal ions (Li^+, Na^+, and K^+) confined in MoS_2 nanoslits on the flow resistance of aqueous solutions under shearing. The nanoslit widths were set at 1.2, 1.6, and 2.0 nm. Analyses of the friction coefficients, density distributions, ionic hydration, and water molecule microstructures led to the following conclusions.

(I) For nanoslits of the same width, the flow resistance sequence is $K^+ < Na^+ < Li^+$.

(II) For the same ionic aqueous solution, as the nanoslit width decreases, the flow resistance increases; *i.e.*, d12 > d16 > d20.

(III) Microstructural analysis of fluid molecules shows that the unique confined spatial distributions of cations and water molecules greatly contribute to confined ionic hydration. Confined ionic hydration causes water molecules in the hydration shell to orient in a specific direction, causing a decrease in the number of HBs. This in

383 coefficient depends on the number of HBs per water molecule; *i.e.*, the greater the
384 extent of HB formation, the lower is the flow resistance.
385
386 **Supplementary material**

387 Supplementary material related to this article can be found at https://dx.doi.org/< >

388 **Acknowledgements**

389 This work was supported by the National Science Foundation of China [21878144,
390 21576130, 21490584 and 21506090], Project of Jiangsu Natural Science Foundation
391 of China (BK20171464), Qing Lan Project, Jiangsu Overseas Visiting Scholar
392 Program for University Prominent Young & Middle-aged Teachers and Presidents,
393 and the State Key Laboratory of Materials-Oriented Chemical Engineering [No.
394 KL15-03 and KL16-01]. We are grateful to the High Performance Computing Center
395 of Nanjing Tech University for supporting the computational resources.

396 **Nomenclature**

397 *Acronyms*

398	HB	hydrogen bond
399	NEMD	non-equilibrium molecular dynamics
400	NPT	the isobaric-isothermal ensemble
401	NVT	the canonical ensemble
402	PC-SAM	phosphorylcholine self-assembled monolayers
403	PMF	the potential of mean force

404

N_{eff}	effective hydration number
N_{HB}	mean number of hydrogen bonds per water molecule
q	charge of atom (e)
R_{min}	the first coordination shell radius (Å)
$U(r_{ij})$	the interaction energy between sites i and j (kcal/mol)
α	orientation angle
ε	Lennard-Jones energy constant (kcal/mol)
$\rho(z)$	density distribution along z-direction in confinement (nm^{-1})
ρ_0	density in bulk (nm^{-1})
σ	Lennard-Jones length constant (Å)
ρ	the water density (kg/m^3)

References

[1] E. Cha, M. D. Patel, J. Park, J. Hwang, V. Prasad, K. Cho and W. Choi, Nat. Nanotech., 2018, 13, 337-344.

[2] X. Zhang, Z. C. Lai, C. L. Tan and H. Zhang, Angew. Chem. Int. Ed, 2016, 55, 8816-8838.

[3] G. Zhang, H. J. Liu, J. H. Qu and J. H. Li, Energy Environ. Sci., 2016, 9, 1190-1209.

[4] X. A. Cao, X. H. Gan, Y. T. Peng, Y. X. Wang, X. Z. Zeng, H. J. Lang, J. N. Deng and K. Zou, Nanoscale, 2017, 10, 378-385.

[5] A. B. Farimani, K. Min and N. R. Aluru, Acs Nano, 2014, 8, 7914-7922.

[6] K. Liu, J. D. Feng, A. Kis and A. Radenovic, Acs Nano, 2014, 8, 2504-2511.

[7] M. Acerce, D. Voiry and M. Chhowalla, Nat. Nanotech., 2015, 10, 313-318.

[8] M. Heiranian, A. B. Farimani and N. R. Aluru, Nat. Commun., 2015, 6,1-6.

[11] Z. X. Luo, Y. Z. Xing, Y. C. Ling, A. Kleinhammes and Y. Wu, Nat. Commun., 2015, 6,1-8.

[12] H. Sakuma, K. Otsuki and K. Kurihara, Phys. Rev. Lett., 2006, 96, 046104.

[13] Gaisinskaya-Kipnis, L. R. Ma, N. Kampf and J. Klein, Langmuir, 2016, 32, 4755-4764.

[14] J. Klein, Friction, 2013, 1, 1-23.

[15] L. Z. Zhang and S. Y. Jiang, J. Chem. Phys., 2003, 119, 765-770.

[16] C. L. Wang, B. H. Wen, Y. S. Tu, R. Z. Wan and H. P. Fang, J. Phys. Chem. C, 2015, 119, 11679-11684.

[17] Y. He, S. F. Chen, J. C. Hower, M. T. Bernards and S. Y. Jiang, J. Chem. Phys., 2007, 127, 084708.

[18] J. E. Black, C. R. Iacovella, P. T. Cummings and C. McCabe, Langmuir, 2015, 31, 3086-3093.

[19] A. Z. Summers, C. R. Iacovella, M. R. Billingsley, S. T. Arnold, P. T. Cummings and C. McCabe, Langmuir, 2016, 32, 2348-2359.

[20] A. Z. Summers, C. R. Iacovella, P. T. Cummings and C. McCabe, Langmuir, 2017, 33, 11270-11280.

[21] P. Wang, M. Wang, F. Liu, S. Ding, X. Wang, G. Du, J. Liu, P. Apel, P. Kluth, C. Trautmann and Y. Wang, Nat. commun., 2018, 9, 569.

[22] R. K. Joshi, P. Carbone, F. C. Wang, V. G. Kravets, Y. Su, I. V. Grigorieva, H. A. Wu, A. K. Geim and R. R. Nair, Science, 2014, 343, 752-754.

[23] J. Abraham, K. S.Vasu, C. D. Williams, K. Gopinadhan, Y. Su, C. T. Cherian, J. Dix, E. Prestat, S. J. Haigh, I. V. Grigorieva, P. Carbone, A. K. Geim and R. R. Nair, Nat. Nanotechnol., 2017, 12, 546-550.

[24] C. D. Williams, J. Dix, A. Troisi and P. Carbone, J. Phys. Chem. Lett., 2017, 8, 703-708.

[25] S. Plimpton, J. Computat. Phys., 1995, 117, 1-19.

[26] H. J. C. Berendsen, J. R. Grigera and T. P. Straatsma, J. Phys. Chem., 1987, 91, 6269-6271.

[27] W. L. Jorgensen, D. S. Maxwell and J. Tirado-Rives, J. Am. Chem. Soc., 1996, 118, 11225-11236.

[28] V. Varshney, S. S. Patnaik, C. Muratore, A. K. Roy, A. A. Voevodin and B. L. Farmer, Comput. Mater. Sci., 2010, 48, 101-108.

[30] Y. M. Zhang, Y. D. Zhu, Z. R. Li, Y. Ruan, L. C. Li, L. H. Lu and X. H. Lu, Fluid Phase Equilib., 2016, 430, 169-177.

[31] G. J. Martyna, D. J. Tobias and M. L. Klein, J. Chem. Phys., 1994, 101, 4177-4189.

[32] R. W. Hockney and J. W. Eastwood, SIAM Rev., 1983, 25, 425-426.

[33] Y. D. Zhu, L. Z. Zhang, X. H. Lu, L. H. Lu and X. M. Wu, Fluid Phase Equilib., 2014, 362, 235-241.

[34] Y. D. Zhu, Y. M. Zhang, Y. J. Shi, X. H. Lu, J. H. Li and L. H. Lu, J. Chem. Eng. Data, 2016, 61, 4023-4030.

[35] Y. S. Leng, Langmuir, 2012, 28, 5339-5349.

[36] G. Mogami, M. Suzuki and N. Matubayasi, J. Phys. Chem. B, 2016, 120, 1813-1821.

[37] J. B. Peng, D. Y. Cao, Z. L. He, J. Guo, P. Hapala, R. Z. Ma, B. W. Cheng, J. Chen, W. J. Xie, X. Z. Li, P. Jelinek, L. M. Xu, Y. Q. Gao, E. G. Wang and Y. Jiang, Nature, 2018, 557, 701-705.

[38] J. Zhou, X. H. Lu, Y. R. Wang and J. Shi, Fluid Phase Equilib., 2002, 194, 257-270.

[39] Q. Shao, J. Zhou, L. H. Lu, X. H. Lu, Y. Zhu and S. Y. Jiang, Nano Lett., 2009, 9, 989-994.

[40] Y. D. Zhu, Y. Ruan, Y. M. Zhang, L. H. Lu and X. H. Lu, Mol. Simulat., 2016, 42, 784-798.

[41] M. Antognozzi, A. D. L. Humphris and M. J. Miles, Appl. Phys. Lett., 2001, 78, 300-302.

[42] M. Hussain and J. Anwar, J. Am. Chem. Soc., 1999, 121, 8583-8591.

[43] P. Fenter and N. C. Sturchio, Prog. Surf. Sci., 2004, 77, 171-258.

[44] D. Eisenberg and W. Kauzmann, The structure and properties of water, Oxford University Press, Oxford, 12th edn, 2005.

[45] F. Franks, Water A Comprehensive Treatise, Plenum Press, US, 1st edn, 1972.

[46] Luzar and D. Chandler, Nature, 1996, 379, 55-57.

[47] B. Hribar, N. T. Southall, V. Vlachy and K. A. Dill, J. Am. Chem. Soc., 2002, 124, 12302-12311.

[48] K. Soper and K. Weckstrom, Biophys. Chem., 2006, 124, 180-191.

121, 5669-5678.

Figure captions

Fig. 1. Model of ionic aqueous solution confined in a MoS_2 slit. The yellow and blue atoms represent the sulfur and molybdenum atoms in MoS_2 molecules, respectively. The red and white atoms represent the oxygen and hydrogen atoms in water molecules, respectively. The green and pink atoms represent the cation and anion atoms, respectively.

Fig. 2. The friction coefficients of Li^+, Na^+ and K^+ aqueous solutions confined within MoS_2 slits with different widths. The d12, d16 and d20 on the horizontal axis represent the slits with 1.2, 1.6 and 2.0 nm widths, respectively.

Fig. 3. Density profiles of water molecules in Li^+, Na^+ and K^+ aqueous solutions confined in d12, d16 and d20 along the *Z* direction. The red dashed lines represent the surfaces of slits.

Fig. 4. *X*−*Z* planar density distributions of Li^+, Na^+ and K^+ confined in d12, d16 and d20. The horizontal coordinates (bottom) represent the lateral distance along *X* direction of slit. The density distributions of water molecules (light blue curve) was drawn together in order to illustrate the relative position of cation distribution. The horizontal coordinates (upper) represent the magnitude for water density profiles, respectively.

Fig. 5. Average effective hydration number of Li^+, Na^+ and K^+ confined in d12, d16 and d20. The black star represents the effective hydration number of the ions in bulk. The inset is a schematic of the orientation angle α of a water molecule around a cation.

Fig. 6. Number of hydrogen bond per water molecule in Li^+, Na^+ and K^+ aqueous solutions confined within d12, d16 and d20. The dashline represents the value of pure

533 **Table captions**

534 **Table 1.** Force field parameters used in this work.

535 **Table 2.** The *Z*-ranges of Li^+, Na^+ and K^+ confined in d12, d16 and d20

536

537 **Table of Contents Graphic**

Effects of ionic hydration and hydrogen bonding on flow resistance of ionic aqueous solutions confined in molybdenum disulfide nanoslits: Insights from molecular dynamics simulations

Yumeng Zhang [a], Wei Zhu [a], Jiahui Li [a], Yudan Zhu [a,*], Anran Wang [a], Xiaohua Lu [a], Wei Li [b], Yijun Shi [c]

538 For Table of Contents use only

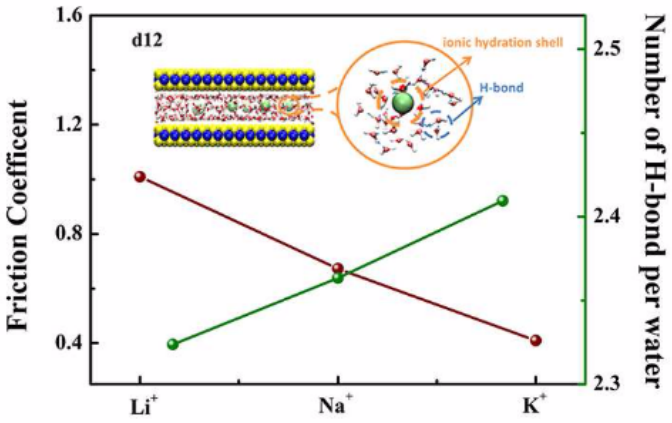

539